International Journal of Hydrogen Energy 281 (2026) 157997

Contents lists available at ScienceDirect

International Journal of Hydrogen Energy

journal homepage: www.elsevier.com/locate/he

Mitigation of ammonia slip through fuel staging in plasma assisted ammonia swirl burners

Ziyu Wang *, B. Aravind **, Syed Mashruk, Agustin Valera-Medina

College of Physical Sciences and Engineering, Cardiff University, Wales, CF24 3AA, UK

ARTICLE INFO

Keywords:
Net zero carbon
Stage combustion
Hydrogen
Plasma assisted combustion
Emission

ABSTRACT

Previous studies have shown that applying gliding arc plasma (GAP) on the ammonia (NH_3) side can reduce NO_x emissions but may increase NH_3 slip under fuel-rich conditions. Therefore, a strategy is needed to minimize both NO_x and NH_3 slip. This study investigates the synergistic effects of fuel staged combustion and GAP assistance on NH_3-air flame systems to mitigate NH_3 slip while maintaining low NOx emissions. A detailed parametric study is conducted by varying secondary air and NH_3 injection ratios to identify optimal emission conditions, complemented by combustion optical diagnostics. Results indicate that fuel staging combined with GAP enhances flame stability, improves fuel-air mixing, and promotes complete NH_3 reaction, achieving NH_3 emissions below 100 ppm and 25-54% reduction in NOx. While GAP effectively reduces NO_x, it may slightly increase N_2O (~10 ppm) under fuel-rich conditions due to enhanced $NH + NO = N_2O + H$ reactions and partial inhibition of N_2O reduction. Furthermore, GAP-assisted fuel staged combustion significantly enhances NH_3 decomposition and radical formation (NH_2*, OH*), strengthening reaction intensity and combustion stability under fuel-rich conditions. These findings demonstrate that the integration of fuel staging and GAP provides an effective strategy for optimizing emissions in NH_3 combustion systems.

Abbreviations and symbols

Abbreviation	Definition
GAP	Gliding arc plasma
LBO	Lean blowout
RBO	Rich blowout
PSD	Power spectral density
RMS	Root mean square
FS	Fuel staging
AS	Air staging
WP	With plasma
NP	No plasma
Symbol	**Definition**
ϕ_g	Global equivalence ratio
NH_2*	Electronically excited NH_2 radical
OH*	Electronically excited OH radical

1. Introduction

Hydrogen (H_2) is widely recognized as a promising carbon-free fuel due to its high reactivity and zero carbon emissions [1,2]. However, its low volumetric energy density and challenges associated with storage and transportation have motivated increasing interest in alternative hydrogen carriers. As a hydrogen carrier, NH_3 offers advantages in terms of storage and transportation while retaining the potential for carbon-free energy conversion. As a carbon-free fuel with well-established production and transportation infrastructures, has recently attracted significant research interest [3]. However, NH_3 exhibits relatively low laminar flame speed, leading to poor flame stability that requires improvement [4,5]. Unlike traditional hydrocarbon fuels, a major disadvantage of using NH_3 as a fuel is its tendency to produce nitrogen oxides (NO_x) during combustion, due to the nitrogen content in NH_3 [6,7].

Active control of NH_3 flames has got considerable attention due to its potential significance in improving combustion efficiency and stability. Among various control strategies, the use of plasma-assisted techniques has recently emerged as a promising approach for regulating flame behaviour [8–13]. Plasma has been demonstrated to effectively enhance ignition performance and flame stabilization across a wide range of

* Corresponding author.
** Corresponding author.
E-mail addresses: Wang6@cardiff.ac.uk (Z. Wang), BalakrishnanA4@cardiff.ac.uk (B. Aravind).

https://doi.org/10.1016/j.ijhydene.2026.157997
Received 8 June 2026; Received in revised form 3 October 2026; Accepted 5 October 2026
Available online 6 October 2026
0360-3199/© 2026 The Authors. Published by Elsevier Ltd on behalf of Hydrogen Energy Publications LLC. This is an open access article under the CC BY license (http://creativecommons.org/licenses/by/4.0/).

combustion systems [14]. These findings indicate that plasma offers distinctive advantages in promoting the combustion characteristics of NH_3 flames. Various plasma technologies, including nanosecond repetitively pulsed (NRP) [4,8], dielectric barrier discharge (DBD) [15], and gliding arc plasma (GAP) [9,10,16], have been employed to enhance combustion through plasma-induced radical generation and modification of reaction kinetics. These plasma technologies have showed promising effects on ignition and flame stabilization. However, the strong electromagnetic interference associated with NRP can complicate experimental system design, while the effects of DBD on emissions from NH_3 combustion appear to be less favourable. In comparison, GAP provides an extended discharge channel and stronger interaction with the reacting flow, making it particularly suitable for relatively simple continuous-flow combustion systems. For NH_3 combustion, previous studies have shown that GAP can promote flame stabilization and reduce NO_x emissions by modifying the reaction pathways. Specifically, Choe et al. [17] reported that nanosecond repetitively pulsed (NRP) discharges can substantially reduce NO_x emissions. To elucidate the promoting mechanisms of NRP on NH_3-air flames, Sun et al. [11] investigated flame development under NRP-induced conditions on the nanosecond timescale. Tang et al. [18] reported that plasma was observed to enhance NO and NH concentrations in the near field of both NH_3-air and NH_3-H_2-air flames across all equivalence ratios. However, the enhancement of NH was less significant in the NH_3-H_2-air cases. Deng et al. [15] investigated NO_x formation behaviour in Dielectric Barrier Discharge (DBD) using planar laser-induced fluorescence and chemiluminescence to simultaneously detect key intermediate radicals (NO, OH, and NH_2). Their study revealed that the increase in NO primarily arises from the more rapid growth of OH radicals compared with NH_2 radicals. Gliding arc plasma (GAP), has also been explored for its potential to enhance NH_3 combustion [19]. GAP has exhibited notable capability in reducing NOx emissions through the application of an external electric field [20,21]. This approach offers a structurally simple and cost-effective configuration, as it requires only the installation of an electrode at the gas inlet, making it particularly attractive for industrial applications. Regarding emission characteristics, Aravind et al. [20] observed substantial NO reduction in partially premixed NH_3-air flames at low plasma power, where the plasma interacted exclusively with the NH_3 stream. Furthermore, Wang et al. [21] examined GAP effects on air-stratified NH_3 flames, and through measurements of NH_2* and OH* radicals, they provided preliminary interpretations of NO_x variation under plasma activation. Previous investigations have demonstrated that the effectiveness of GAP in mitigating NOx emissions is predominantly observed under lean-burn conditions ($\phi < 0.9$). In contrast, at stoichiometric ($\phi = 1$) and rich conditions, increased NH_3 slip is often observed [20]. In summary, GAP shows significant advantages in actively regulating and enhancing NH_3 combustion. However, the substantial NH_3 slip occurring under fuel-rich conditions remains a critical issue that must be addressed. The presence of unburned NH_3 not only compromises combustion efficiency but also poses environmental and health risks owing to its intrinsic toxicity. Therefore, minimizing unburned NH_3 emissions is a critical challenge in NH_3-based combustion systems, requiring optimized combustion strategies, improved catalyst design, and effective exhaust after-treatment technologies to ensure both high efficiency and low environmental impact [22,23].

Rahmani et al. [22] demonstrated that under moderate or intense Moderate or Intense Low-oxygen Dilution (MILD) combustion, the distributed reaction zone and reduced peak temperature provide an effective pathway for suppressing NO_x formation. When the hydrogen fraction was adjusted to an optimal trade-off level, NH_3 slip was reduced by 50%, while NO increased by only 12 ppm, and the MILD combustion regime was maintained. However, reducing NH_3 slip under specific condition places significant constraints on the hydrogen fraction and burner configuration, leading to limited operational flexibility. Therefore, recent research has increasingly favoured staged combustion as an effective strategy for mitigating NH_3 slip across a broader range of operating conditions. According to Liu et al. [24], effective NO_x abatement is attainable exclusively via the thermal $DeNO_x$ route under near-stoichiometric conditions. This outcome results from the intrinsically limited low-NO_x/NH_3 emission window during the primary combustion stage, which promotes lean NH_3/H_2 combustion, followed by the NH_3-to-NO conversion penalty in the secondary stage. Moreover, employing a staged injection strategy in the combustion chamber facilitates thorough mixing between NH_3 and air, which effectively mitigates a NH_3 slip [25,26]. Wang et al. [23] investigated the NH_3/CH_4/air flame under fuel staged combustion and found that increasing the residence time in the primary reaction zone while lowering the temperature in the secondary reaction zone can effectively reduce NO and N_2O emissions. However, excessively low temperatures in the secondary reaction zone may lead to significant N_2O formation and unburned NH_3 slip. Based on the above discussion, the present work integrates a staged combustion strategy with GAP-assisted combustion to alleviate the pronounced NH_3 slip observed under rich conditions, while maintaining low NO_x emissions.

Therefore, a detailed experimental analysis was performed with varying secondary air and NH_3 injection ratios to identify the optimal emission region under GAP combined with fuel staging/air staging (FS/AS) strategy. To the best of the authors' knowledge, this is the first work of the kind combining FS in NH_3 combustion and GAP. The underlying mechanism of the staged combustion-GAP coupling was elucidated through combustion optical diagnostics, with particular focus on the generation of intermediate species. Kinetic modelling using a freely chemical reactor network (CRN) model coupled with 0D plasma reactor is performed to elucidate the mechanisms of GAP-assisted FS NH_3 combustion.

2. Experiment setup

2.1. Experimental apparatus

Experimental investigations were conducted using a newly developed GAP-assisted dual-swirl combustor at the Centre of Excellence on Ammonia Technologies (CEAT), Cardiff University. A comprehensive description of the experimental setup is available in our previous works [20,21]. Two co-swirlers with a swirl number of 1.0 each were located 125 mm and 40 mm upstream of the dump plane for the inner and outer swirlers, respectively. NH_3 was introduced through a central lance and injected via the inner swirler, while air was supplied through the outer swirler and discharged at the dump plane. This configuration generally produces a non-premixed flame. The gliding arc plasma was primarily generated in the annular gap between the central lance and a conical electrode, which also functioned as a bluff body. Unlike previous experiments, the present study incorporates improvements in the fuel/air injection configuration. The burner outlet serves as the primary fuel/air injection point, while a secondary tangential fuel/air inlet is positioned 100 mm downstream of the burner exit. In this study, "air staging" (AS) refers to the injection of secondary air downstream of the primary combustion zone, while "fuel staging" (FS) refers to the injection of fuel at multiple locations. The inlet has a diameter of 6.3 mm and is arranged in four tangential directions around the central ring. The tangential injection promotes an extended residence time, allowing for more complete mixing between fuel and oxidizer. GAP was applied exclusively within the central lance of the primary combustion zone, corresponding to the region where the primary NH_3 was injected. The experimental conditions were set as follows: the total NH_3 flow rate was maintained at 28.5 SLPM (corresponding to 6.5 kW total combustion power), and the primary air flow was fixed at 92.5 SLPM (corresponding to $\phi_g = 1.1$ in the absence of secondary air).

A gas analyser (Emerson CT5100) was applied to derive exhaust emissions, including NO, NO_2, N_2O, NH_3, O_2, H_2O. Emissions were measured at a frequency of 1 Hz and then averaged over 2-min intervals. Gas samples were obtained using a 30 mm isokinetic sampling funnel

placed 15 mm downstream from the exit of the quartz tube. To avoid condensation, the sampling line was heated and maintained at 463K. Data from 120 samples at each test point were normalized to a dry gas composition corresponding to 15% O_2.

Emission measurements were conducted under three operating conditions:

(1) Secondary NH_3 = 0 SLPM, secondary air = 0-30 SLPM.
(2) Secondary NH_3 = 1.4S LPM (5% of total NH_3), secondary air = 0-20 SLPM.
(3) Secondary NH_3 = 0.7-4.3 SLPM (2.5-15% of total NH_3), secondary air = 5 SLPM.

The details can be found in Table 1.

In addition, high-speed imaging was employed to capture NH_2* and OH* chemiluminescence in the primary flame zone (the first stage), using bandpass filters: 309 nm (±10 nm FWHM), and 630 nm (±10 nm FWHM). For each condition, 200 frames were recorded with a LaVision high speed camera. The chemiluminescence intensity distribution was derived using three processing steps: time-averaging, background subtraction, and Abel transformation. While emission spectroscopy was conducted in the secondary stage combustion region to analyse the reaction characteristics. An AvaSpec-ULS spectrometer equipped with a UV/visible optical fibre was positioned 25 mm above the secondary injector. At a working distance of 100 mm, the probe collects light from a region approximately 2-3 mm in diameter, enabling localized spectral measurements within the 30 × 38 mm^2 measurement area. The measured spectrum was mainly concentrated in the range of 300-900 nm due to the emission wavelengths of the dominant excited radicals [10] and the sensitivity characteristics of the detector.

2.2. Numerical methodology

The details of this work on a plasma-assisted FS combustion model are shown in Fig. 1. A PAC model coupling ZDplaskin with Chemkin is introduced for analysis [27–29]. The mechanism contains can be found in our previous work [28]. In the present experiment, both the plasma power (110 W) and the combustion power (6.5 kW) were maintained consistent with those used in previous studies [20]. The computational domain is divided into the ionization and external regions, based on the voltage–current characteristics. The ionization region, with high electron density, drives active electronic reactions, while the external region primarily involves reactions of stable intermediates. It is noteworthy that under conditions without plasma, the fuel injected in the primary stage consists of pure NH_3 rather than gas after discharge.

The model setup for FS combustion follows the approach of Wang et al. [23]. Within each stage, one perfectly stirred reactor (PSR), and one plug flow reactor (PFR) are employed, with relevant parameters defined according to the actual burner geometry. The physical sizes of two PFRs are 100 mm (primary) and 200 mm (secondary) in length and 76 mm in diameter. The residence time in each reactor was self-consistently calculated based on the flow rate and reactor volume. The gas inlet conditions were set to a temperature of 300 K and a pressure of 1atm (ambient pressure). In the path flux analysis, up to 10 species were selected, covering the complete pathway from NH_3 to NO,

Table 1
Flow parameters of the gases entering the combustion chamber.

Gas	Flow rate (SLPM)	V (m/s)	Density (kg/m^3)	Dynamic viscosity (Pa·s)	Reynolds number ($\times 10^3$)
NH_3	24.2-28.5	2.15-2.49	0.705	9.8×10^{-6}	2.45-2.93
Air	92.5	10.12 T	1.184	1.85×10^{-5}	9.50

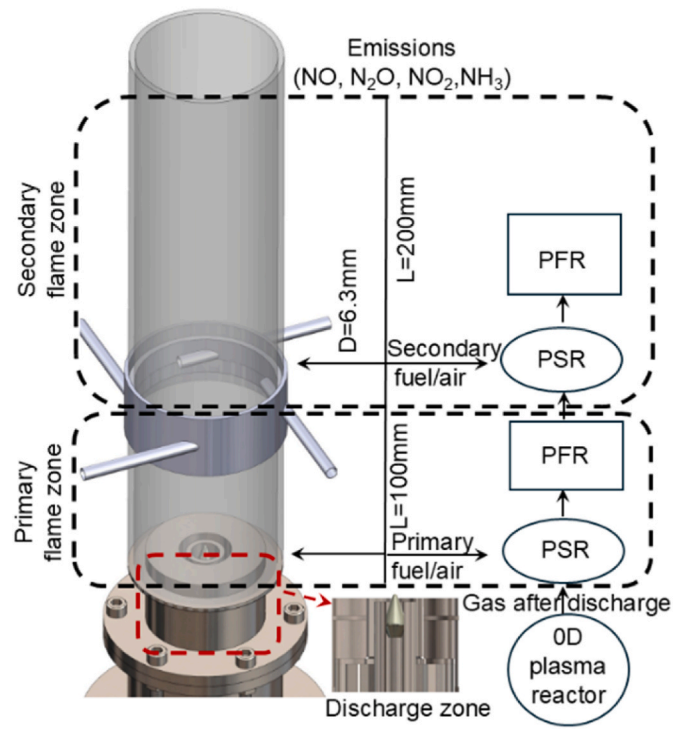

Fig. 1. Schematics of GAP assisted FS combustor and plasma-assisted FS combustion chemical reactor network (CRN) model.

with a minimum correlation coefficient of 0.01 based on the relative rate of production (ROP). The normalization of ROP (Rate of Production) is performed by dividing the rate coefficient of each reaction by the absolute value of the maximum rate coefficient. Negative values represent the consumption of NO and positive values indicate the production of NO.

3. Result and discussion

3.1. Flame morphology

The flame morphology of FS NH_3 combustion under plasma-assisted conditions are shown in Fig. 2.

Flame morphology analysis in Fig. 2 indicates that FS induces multiple fine jet structures in the secondary zone, becoming pronounced at a secondary NH_3 content of 10%. The tangential injection strategy appears to improve fuel-air mixing, leading to a more uniform flame distribution along the quartz tube. This effect reduces the rapid entrainment of unburned NH_3 driven by thermal buoyancy, ensuring more complete combustion in the secondary zone [25]. GAP application effectively stabilizes the lifted flame near the combustor exit, where the arc appears to bridge the fuel jet and flame front [10]. This configuration likely enhances the transport of active radicals from the primary to the secondary combustion zone, thereby extending the radical-driven acceleration of reactions in the lower primary flame region. Consequently, GAP facilitates flame stabilization and promotes more efficient energy release and radical propagation throughout the staged combustion process.

3.2. Emission characteristics

Emissions (NO, NO_2, N_2O and NH_3) are measured with different FS/AS strategies in GAP. The global equivalence ratio (ϕ_g) is introduced as a reference to characterize the overall fuel-lean or fuel-rich condition of the flame, as shown in Fig. 3.

For the emission characteristics under the condition of secondary air

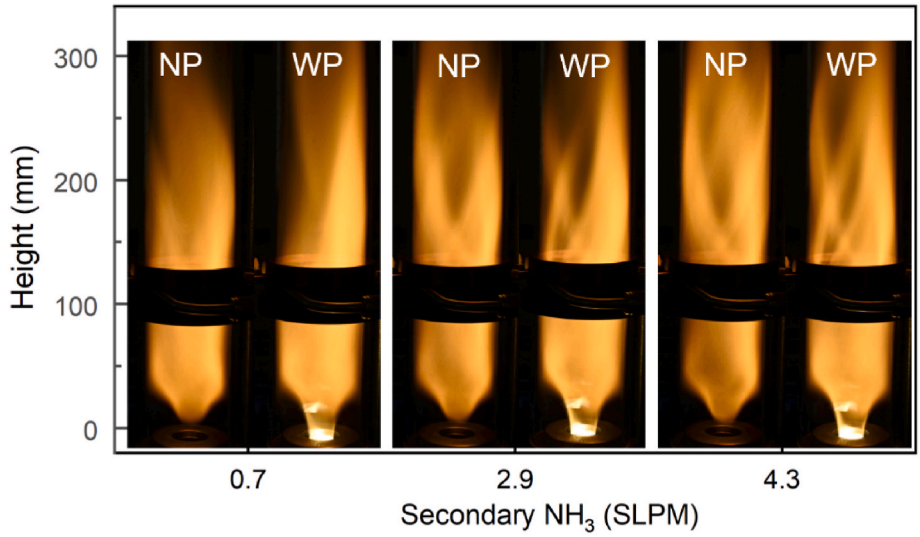

Fig. 2. Variation of flame morphology. (FS combustion with plasma (WP) and no plasma (NP)).

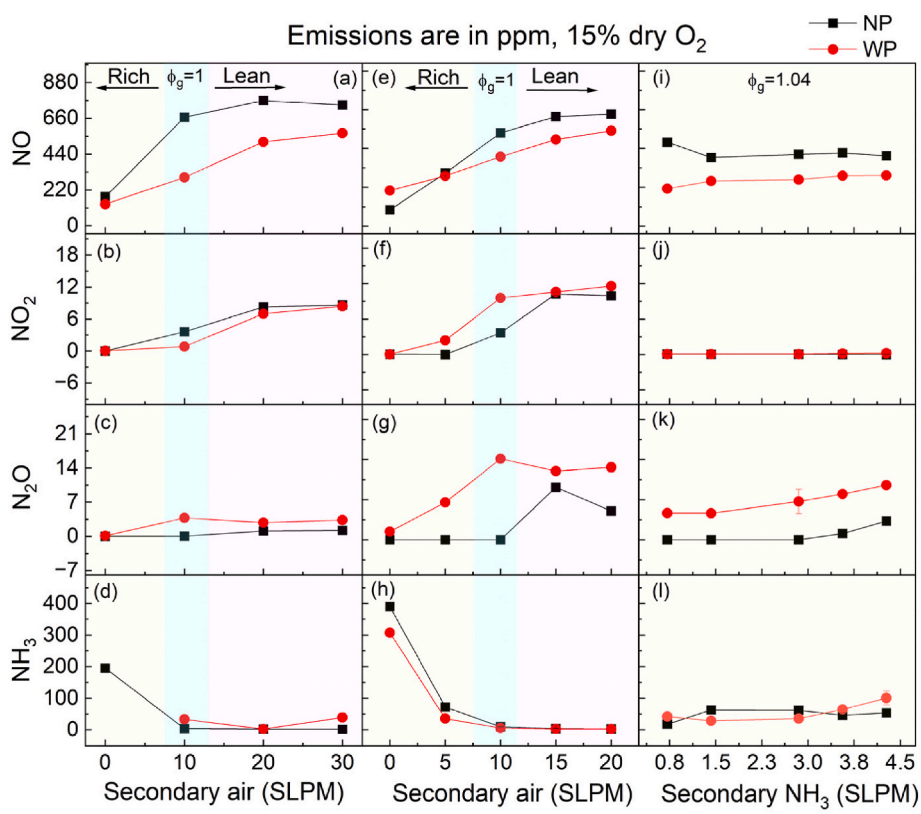

Fig. 3. Emissions of FS/AS combustion: (a)-(d) Secondary NH_3 = 0 SLPM, (e)-(h) Secondary NH_3 = 1.4 SLPM, (i)-(l) Secondary air = 5 SLPM.

injection only, as shown in Fig. 3(a)–(d), the injection of secondary air appears to primarily influence the overall equivalence ratio, thereby affecting the emission behaviour. Notably, a peak in NO formation is observed around $\phi_g = 0.8$. This behaviour can be attributed to the competition between NO formation and consumption pathways. Under richer conditions, the limited availability of oxidizing species suppresses the oxidation of NHx intermediates toward NO. As the mixture becomes leaner, enhanced NH3 oxidation promotes the formation of NO through nitrogen-containing intermediates. However, with further air addition, the decreasing flame temperature and changes in the radical pool can limit NO formation, resulting in a peak around $\phi_g = 0.8$. This observation is also consistent with our previous experimental findings [14]. The application of GAP significantly reduces NOx under lean combustion conditions; however, it still exacerbates NH_3 slip under rich conditions (secondary air = 0 SLPM), leading to readings beyond the measurable range (>2000 ppm). These observations are consistent with our previous findings [20]. In contrast, the N_2O concentration exhibits only slight variations, remaining below 10 ppm, compared with the previous value of 0 ppm. When the secondary NH_3 flow was set to 1.4 SLPM, the overall NOx emissions decreased, and NH_3 slip under fuel-rich conditions was significantly mitigated in Fig. 3(e)–(h). Under the same fuel/air ratio, the FS injection strategy achieved approximately

a 10% reduction in NO emissions. Notably, this reduction in NO_x was not accompanied by an increase in NH_3 concentration; for instance, with a secondary air flow of 5 SLPM, NH_3 levels remained as low as 35 ppm. In the absence of secondary air, the application of GAP promoted greater participation of NH_3 in the reaction, resulting in a 25% reduction in NH_3 emissions compared with the scenario without GAP. However, this was associated with an increase in NO emissions from 104 ppm to 228 ppm. Increasing the air flow further enhanced the NO reduction effect of GAP, albeit with a slight rise in N_2O emissions.

Therefore, a secondary air flow of 5SLPM was selected, corresponding to slightly fuel-rich conditions ($\phi_g = 1.04$). The emissions corresponding to different secondary NH_3 flows under these conditions are presented in Fig. 3(i)–(f). It can be observed that under different secondary NH_3 conditions, NH_3 emissions remained below 100 ppm, indicating that the FS strategy effectively suppressed unreacted NH_3. Simultaneously, in synergy with GAP, NOx emissions were reduced by 25-54%, resulting in overall emissions of 246-338 ppm. This reduction was particularly pronounced at secondary NH_3 levels of 2.5-10%, which may be attributed to the local equivalence ratio in the sub-flame zone approaching unity, allowing the secondary NH_3 to react more completely. However, GAP also led to approximately 10 ppm of N_2O emissions. According to Alnasif et al. [30], in the fuel-rich zone, the primary formation pathway of N_2O is $NH + NO \rightarrow N_2O + H$, whereas its reduction is mainly governed by the reaction $N_2O + H \rightarrow N_2 + OH$. When GAP generates additional NH in the primary combustion zone that enters the secondary zone, the reaction with NO promotes further N_2O formation, resulting in higher emissions. Moreover, the partial N_2 introduced with the secondary air inhibits the reduction pathway of N_2O in the secondary region. Nevertheless, the overall N_2O emissions remained below 20 ppm, which falls within a relatively low range.

Overall, the emission characteristics demonstrate that the secondary injection strategy combined with FS combustion can effectively balance NOx reduction and NH_3 slip control, achieving a 25-54% reduction in NOx emissions while maintaining NH_3 slip (<100 ppm) and N_2O emissions (<20 ppm) within acceptable limits. In the FS configuration, the introduction of secondary NH_3 further modifies the local equivalence ratio and nitrogen conversion pathways. When secondary NH_3 accounts for approximately 5-10% of the total NH_3 input, relatively low NOx emissions can be achieved while maintaining NH_3 slip below 100 ppm. These results suggest that the benefit of fuel staging arises from regulating the subsequent conversion of NH_3-derived nitrogen species in the secondary combustion zone, rather than simply increasing NH_3 consumption in the primary zone.

3.3. Effects on the key intermediate species

To understand the effect of key species on emission characteristics under the influence of GAP and FS, simultaneous chemiluminescence imaging of NH_2* and OH* is captured for different secondary NH_3 in primary flame zone. Meanwhile, the average intensity values were extracted from each image for more intuitive comparison, as shown in Fig. 4.

Chemiluminescence imaging and quantitative analysis indicate that plasma significantly enhances the formation of key reactive intermediates, NH_2* and OH*, compared to no plasma conditions [21]. Under plasma, NH_2* intensity is approximately 80-100% higher than no plasma cases across all secondary NH_3 flows in Fig. 4 (a), suggesting increased concentration and stability of this intermediate, while OH* intensity increases by 60-120% in Fig. 4 (b), particularly at higher NH_3 flows, highlighting plasma-promoted radical generation. Specifically, the NH_2* signal with plasma shows broader distribution along the flame axis, suggesting increased availability of intermediate radicals, which may facilitate more complete NH_3 conversion. Similarly, the OH* images demonstrate that plasma assistance significantly intensifies the high-temperature reaction zone, leading to enhanced hydrogen and oxygen radical formation, which is critical for promoting NH_3 oxidation and NO_x reduction [20]. With increasing secondary NH_3 flow, NH_2* under plasma decreases slightly (~10%), which can be attributed to the reduced NH_3 flux in the main combustion zone, leading to lower NH_2 production via NH_3 pyrolysis/ionization. OH* increases by up to 30%, indicating enhanced radical availability. The gradual increase of OH* intensity with increasing secondary NH_3 under with plasma conditions implies enhanced oxidation activity. Conversely, the OH* intensity under no plasma cases remains low and nearly constant, highlighting the limited radical generation in conventional combustion and the corresponding lower reaction rates. These enhancements promote NH_3-NO reactions and accelerate the consumption of nitrogen oxide intermediates, explaining the observed reduction in NH_3 slip and

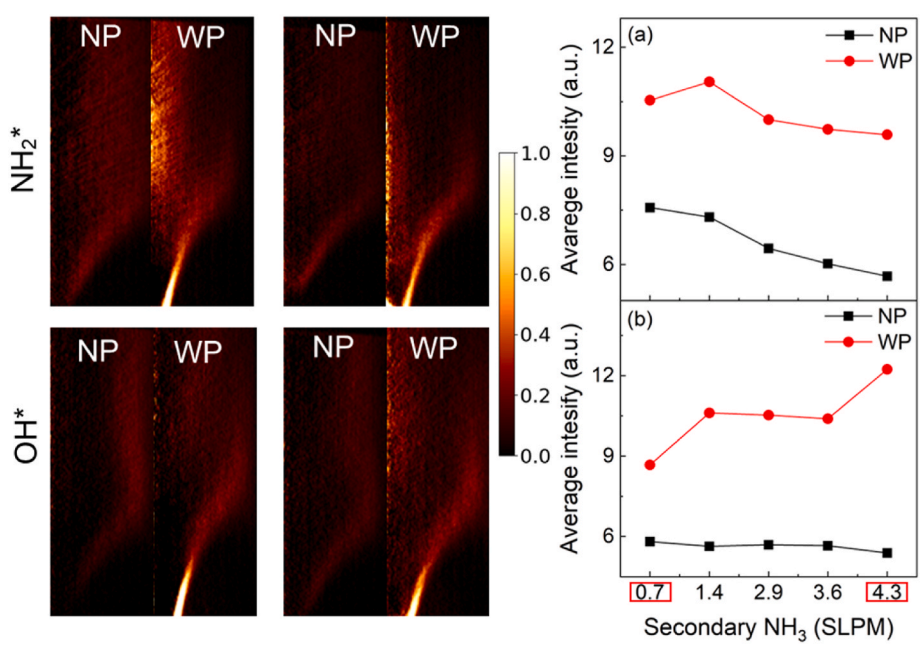

Fig. 4. Abel-deconvoluted OH* and NH_2* chemiluminescence images at secondary NH_3 = 0.7 SLPM (left) and 4.3 SLPM (right) (secondary air = 5SLPM) and average intensity of (a) NH_2*, (b) OH*.

reduction of NO_x conversion efficiency under plasma-assisted conditions. The combination of enhanced radical density and more uniform radical distribution contributes to more complete NH_3 oxidation, consistent with the previously observed reductions in NH_3 slip and simultaneous NO_x control.

As illustrated in Fig. 5, spectrum measurements in the secondary flame zone are conducted, with particular emphasis on the comparative effects of the GAP and FS.

In Fig. 5 (a), as the secondary NH_3 flow rate increases from 0.7SLPM to 4.3SLPM, the overall emission intensity markedly rises, particularly in the wavelength range of 600-850 nm (NH_2 band) [21]. the peaks occurred at 734 nm in all cases in NH_2 (α band, $^2A_1$-$^2B_1$) [21]. This enhancement is mainly attributed to the increased concentrations of active radicals such as OH*, NH*, which are typical indicators of stronger combustion reactions. Corresponding to Fig. 2, when the secondary fuel fraction is 4.3 SLPM, a large amount of "branched flames" is observed in the secondary combustion zone. The higher secondary fuel supply intensifies the local fuel-rich zone and promotes subsequent reburning reactions, leading to a higher temperature and a more active flame region. Therefore, the FS combustion strategy effectively strengthens the reaction intensity and improves combustion stability under fuel-rich conditions. The characteristics with and without plasma assistance are compared in Fig. 5 (b). When plasma is applied, the chemiluminescence intensity across the entire spectrum significantly increases compared to the no plasma cases, although the spectral shape remains similar. The plasma introduces high-energy electrons and reactive species (e.g., N, H, and O radicals) [31], which accelerate NH_3 decomposition and enhance radical formation. Consequently, the reaction rate and combustion completeness are improved.

3.4. Reaction mechanism analysis

The species density of main products in NH_3 flow under GAP discharge are shown in Fig. 6.

In the early stage immediately after plasma ignition (10^{-9}-10^{-7} s), the densities of H and NH_2 increase rapidly, while the density of NH_3 remains nearly constant. This behaviour implies that the dominant processes during this stage are electron-impact excitation and dissociation of NH_3 molecules. The primary reactions responsible for the rapid

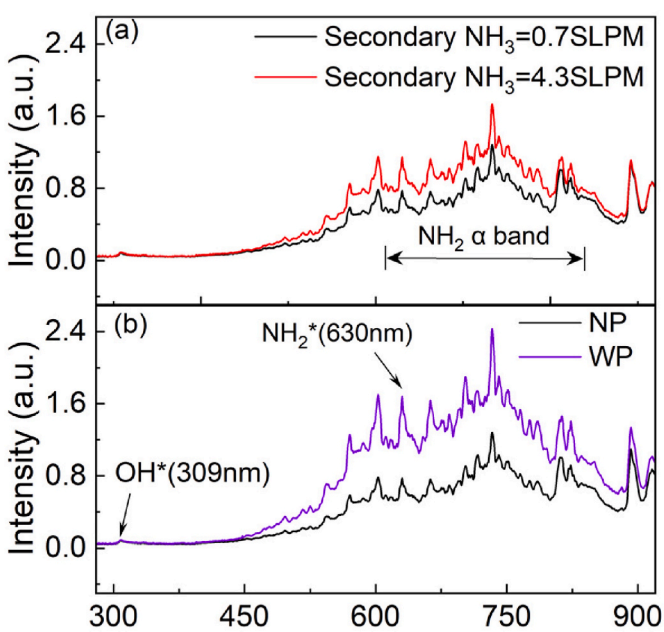

Fig. 5. Spectrum of FS NH_3-air combustion in GAP. (a) different secondary NH_3, (b) With plasma and no plasma.

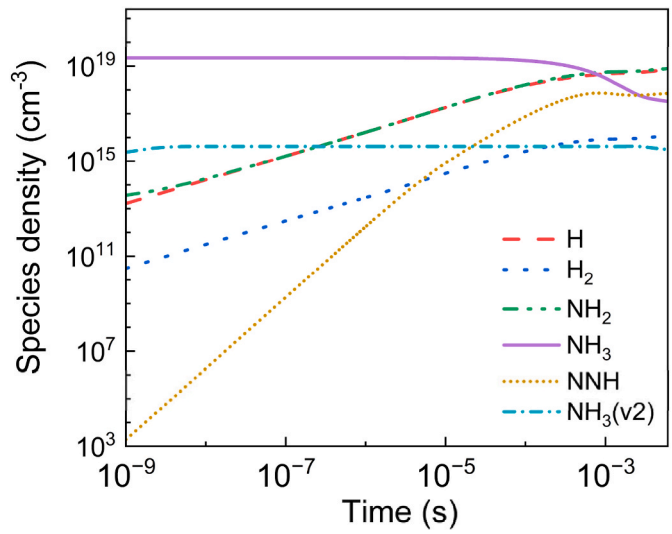

Fig. 6. Effect of NH_3 flow on key species densities in GAP discharge.

formation of radicals are vibrational excitation: $E + NH_3 \rightarrow E + NH_3(v2)$ (0.118eV), $e + NH_3 \rightarrow e + NH_2 + H$ (5.72eV) [27]. The generation rates of NH_2 and H remain closely correlated throughout the plasma region, which is primarily attributed to the dominant dissociation reaction of NH_3 ($NH_3 \rightarrow NH_2 + H$). Among these processes, vibrational excitation occurs at a lower energy threshold and typically has a larger cross section than direct dissociation. As a result, vibrationally excited NH_3 ($NH_3(v2)$) (0.118 eV) is produced almost instantaneously after the discharge is initiated. The relatively stable density of $NH_3(v2)$ observed in the figure suggests that the rates of vibrational excitation and de-excitation are approximately balanced during this stage. After that period, the density of NH_3 starts to decrease more noticeably, reflecting the cumulative effect of sustained dissociation reactions. At the same time, the densities of H_2 and NNH continue to increase. The main formation of NNH are N_2(v1-8) + H→NNH. The delayed formation of NNH indicates its role as a key intermediate in the N_2 formation pathway.

The combustion analysis combined path flux and rate of production of NO. The reaction pathway fluxes of two flame zones under GAP-assisted FS are shown in Fig. 7.

Based on the path flux analysis presented in Fig. 7(a) and (b), the mechanisms responsible for NO reduction under plasma-assisted staged combustion can be clearly identified by comparing the dominant nitrogen conversion pathways in the no plasma and plasma-assisted cases. In Fig. 7 (a), NH_3 oxidation mainly follows the conventional stepwise dehydrogenation route, where NH_3 is first converted to NH_2 primarily through reactions with OH radicals, followed by successive transformations $NH_2 \rightarrow NH \rightarrow N$ [21]. The generated atomic nitrogen then reacts predominantly with OH to form NO, which constitutes one of the major NO formation pathways in conventional NH_3 combustion. The high flux of the $N + OH \rightarrow NO$ reaction in the primary flame zone indicates that a large fraction of fuel-bound nitrogen is oxidized to NO once atomic N is produced. Consequently, the nitrogen conversion network in the no plasma cases strongly favours NO formation (25.9%), leading to relatively higher NO emissions. In contrast, in Fig. 7 (b), the nitrogen reaction network is significantly altered. Although the initial activation of NH_3 to NH_2 remains dominant, the presence of plasma-generated radicals promotes additional reaction channels involving intermediate species such as tHNNH [32] and NNH [33]. These intermediates introduce an alternative pathway in which nitrogen species are converted directly to N_2 through the sequence $NH_2 \rightarrow$ tHNNH $\rightarrow$ NNH $\rightarrow N_2$ [32], thereby bypassing the formation of atomic N and suppressing the subsequent HNO route. As a result, a portion of fuel nitrogen that would otherwise contribute to NO formation is redirected toward N_2 production. Furthermore, plasma assistance enhances the

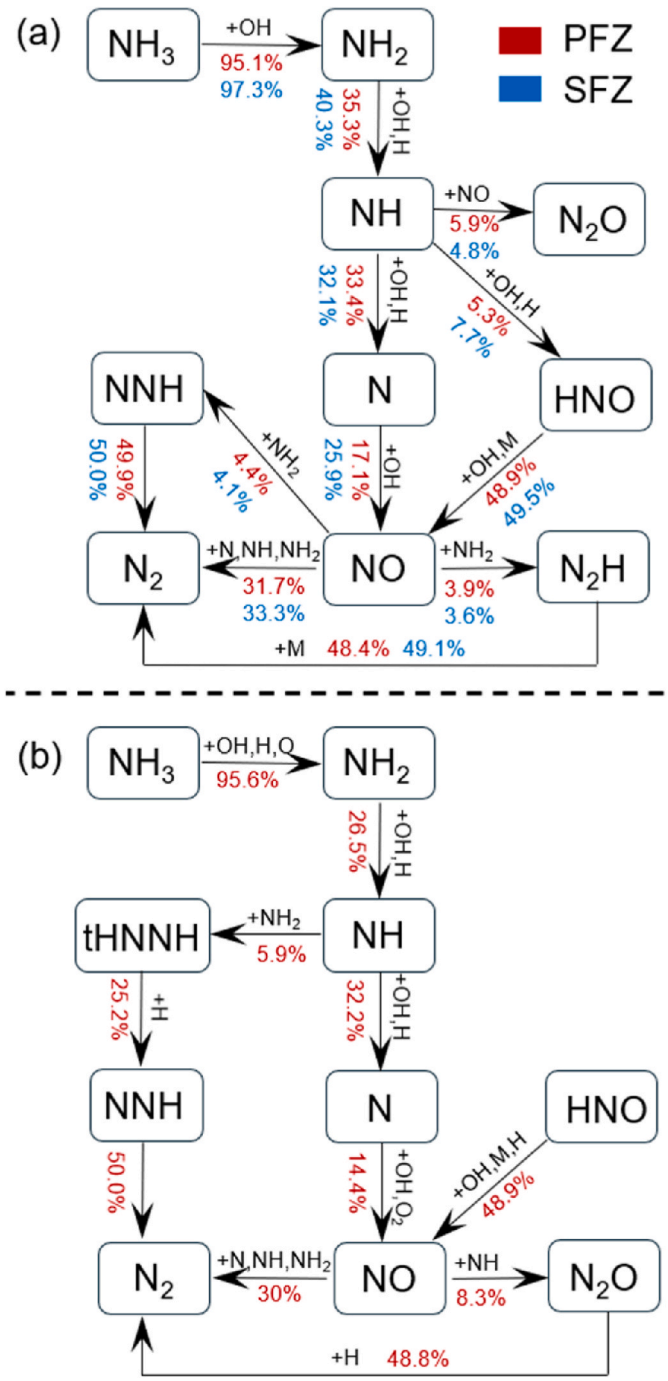

Fig. 7. Path flux of FS combustion in GAP. (a) primary flame zone (PFZ) and secondary flame zone (SFZ) without plasma, (b) primary flame zone with plasma. ($\phi_g = 1.04$, secondary $NH_3 = 1.4$ SLPM, secondary air = 5 SLPM).

generation of reactive radicals, such as H, OH, and NH_x. These radicals modify the reaction environment in both the primary and secondary flame zones. In the staged combustion configuration, the secondary flame zone typically operates under slightly fuel-rich conditions. The elevated concentrations of NH_x radicals can facilitate NO reduction through reactions such as $NO + NH \rightarrow N_2 + OH$ and $NO + NH_2 \rightarrow N_2 + H_2O$. The increased availability of these reducing radicals strengthens the reburning mechanism and promotes the conversion of NO back to N_2. Another possible explanation is related to the effect of secondary injection on the local flame temperature. Wang et al. [23] reported that NO emissions were significantly reduced in the vicinity of the injection location due to the relatively lower flame temperature. Meanwhile, the redistribution of reaction flux away from the N + OH pathway further suppresses thermal and fuel NO formation. Consequently, plasma-induced radical generation and FS substantially restructure the nitrogen chemistry. This restructuring promotes N_2-forming pathways, reduces N-NO conversion, and enhances NO reduction reactions in the secondary flame region. These combined effects ultimately contribute to the observed decrease in NO emissions under plasma assisted staged NH_3 combustion. These synergistic effects ultimately contribute to the observed decrease in NO emissions under plasma-assisted staged NH_3 combustion.

4. Conclusion

The objective of this study is to elucidate whether FS combustion and GAP exhibit synergistic effects in NH_3 flame systems. The principal outcomes obtained from this work are listed below:

1. FS combined with GAP enhances flame stability, improves fuel-air mixing, and promotes complete NH_3 reaction. This can be attributed to the generation of intermediate radicals under plasma excitation, with NH_2* intensity increasing by approximately 80-100% and OH* intensity increasing by 60-120% compared with the no-plasma cases across all secondary NH_3 flow rates.
2. With secondary NH_3 accounting for 5-10% of the total NH_3 input, low NOx emissions can be achieved while maintaining NH_3 slip below 100 ppm. Under different secondary NH_3 injection conditions, NH_3 emissions were maintained below 100 ppm, indicating the effectiveness of the FS strategy in suppressing unreacted NH_3. When coupled with GAP, NOx emissions decreased by 25-54%, resulting in total NOx emissions ranging from 246 to 338 ppm. While GAP effectively reduces NOx, it can slightly increase N_2O (~10 ppm) under fuel-rich conditions. This trade-off attributed to enhanced NH + NO═N_2O + H reactions and partial inhibition of N_2O reduction, highlighting the need to carefully tune secondary NH_3 and air flows. These findings provide useful guidance for the development of FS combustion strategies for emission reduction in NH_3 combustion.
3. GAP-assisted FS combustion enhances NH_3 decomposition and radical formation (NH_2*, OH*), improving reaction intensity, combustion stability under fuel-rich conditions. Meanwhile, the combined effects of plasma-induced radical generation and FS combustion potentially lead to enhanced N_2-forming pathways and suppressed NO formation, ultimately contributing to a significant reduction in NO emissions during plasma-assisted staged NH_3 combustion.

The current secondary air injection strategy is limited to a four-hole injection configuration. Future work could focus on optimizing the secondary air injection location, port geometry, and other parameters to further study in reducing emissions. Coupling this with numerical analysis of the flow field and temperature distribution could help develop an optimal FS strategy to mitigate NH_3 slip under GAP-induced fuel-rich conditions.

CRediT authorship contribution statement

Ziyu Wang: Writing – original draft, Methodology, Investigation, Formal analysis, Data curation. **B. Aravind:** Writing – original draft, Supervision, Methodology, Funding acquisition, Formal analysis, Data curation, Conceptualization. **Syed Mashruk:** Writing – review & editing, Resources. **Agustin Valera-Medina:** Writing – review & editing, Supervision, Resources, Funding acquisition.

Declaration of competing interest

The authors declare that they have no known competing financial interests or personal relationships that could have appeared to influence

the work reported in this paper.

Acknowledgements

This work was supported by the European Union Project CAIPIRI-NH3A, under the GA Number 101191768. Views and opinions expressed are however those of the author(s) only and do not necessarily reflect those of the European Union or CINEA. Neither the European Union nor the granting authority can be held responsible for them. The research was undertaken at Cardiff University's Thermofluids Lab (W/0.17) with invaluable technical support from MR. Jonathan Martin.

References

[1] Kovač A, Paranos M, Marciuš D. Hydrogen in energy transition: a review. Int J Hydrogen Energy 2021;46(16):10016–35. https://doi.org/10.1016/j.ijhydene.2020.11.256. 2021/03/03/.
[2] Li Y, Wang J, Han M, Zhang L, Chen Z, Ma Y. Experimental study of combustion instability and flame dynamics of hydrogen-enriched methane and pure hydrogen swirl flames. Int J Hydrogen Energy 2026;273:157374. https://doi.org/10.1016/j.ijhydene.2026.157374. 2026/09/30/.
[3] Valera-Medina A, Xiao H, Owen-Jones M, David WIF, Bowen PJ. Ammonia for power. Prog Energy Combust Sci 2018;69:63–102. https://doi.org/10.1016/j.pecs.2018.07.001. 2018/11/01/.
[4] Aravind B, Yu L, Lacoste D. Enhancement of lean blowout limits of swirl stabilized NH3-CH4-Air flames using nanosecond repetitively pulsed discharges at elevated pressures. Applications in Energy and Combustion Science 2023;16:100225. https://doi.org/10.1016/j.jaecs.2023.100225. 2023/12/01/.
[5] Valera-Medina A, et al. Premixed ammonia/hydrogen swirl combustion under rich fuel conditions for gas turbines operation. Int J Hydrogen Energy 2019;44(16):8615–26. https://doi.org/10.1016/j.ijhydene.2019.02.041. 2019/03/29/.
[6] Davies J, Mashruk S, Sato D, Mazzotta L, Pugh D, Valera-Medina A. Emissions analyses of humidified cracked ammonia swirling flames. Combust Flame 2025;274:113984. https://doi.org/10.1016/j.combustflame.2025.113984. 2025/04/01/.
[7] Valera-Medina A, Pugh DG, Marsh P, Bulat G, Bowen P. Preliminary study on lean premixed combustion of ammonia-hydrogen for swirling gas turbine combustors. Int J Hydrogen Energy 2017;42(38):24495–503. https://doi.org/10.1016/j.ijhydene.2017.08.028. 2017/09/21/.
[8] Dou JY, Fong AJ, Cenker E, Lacoste DA. Ignition of ultra-lean and highly-diluted hydrogen-air mixtures by bursts of nanosecond repetitively pulsed discharges. Int J Hydrogen Energy 2025;162:150663. https://doi.org/10.1016/j.ijhydene.2025.150663. 2025/08/28/.
[9] Ju R, et al. Stability and emission characteristics of ammonia/air premixed swirling flames with rotating gliding arc discharge plasma. Energy 2023;277:127649. https://doi.org/10.1016/j.energy.2023.127649. 2023/08/15/.
[10] Tang Y, Xie D, Shi B, Wang N, Li S. Flammability enhancement of swirling ammonia/air combustion using AC powered gliding arc discharges. Fuel 2022;313:122674. https://doi.org/10.1016/j.fuel.2021.122674. 2022/04/01/.
[11] Sun J, et al. A comprehensive study on dynamics of flames in a nanosecond pulsed discharge. Part II: plasma-assisted ammonia and methane combustion. Combust Flame 2025;275:114076. https://doi.org/10.1016/j.combustflame.2025.114076. 2025/05/01/.
[12] Sun J, Tang Y, Li S. Plasma-assisted stabilization of premixed swirl flames by gliding arc discharges. Proc Combust Inst 2021;38(4):6733–41. https://doi.org/10.1016/j.proci.2020.06.223. 2021/01/01/.
[13] Zou S, et al. Synergistic NOX reduction in plasma-assisted ammonia-coal combustion: roles of staging ratio and injection position. Int J Hydrogen Energy 2026;244:155612. https://doi.org/10.1016/j.ijhydene.2026.155612. 2026/06/22/.
[14] Popov NA, Starikovskaia SM. Relaxation of electronic excitation in nitrogen/oxygen and fuel/air mixtures: fast gas heating in plasma-assisted ignition and flame stabilization. Prog Energy Combust Sci 2022;91:100928. https://doi.org/10.1016/j.pecs.2021.100928. 2022/07/01/.
[15] Deng K, et al. Addressing NOX formation mechanisms of NH3/H2 dual-fuel flame under DBD plasma-assisted combustion resolved by intermediate radicals analysis. Int J Hydrogen Energy 2024;96:938–51. https://doi.org/10.1016/j.ijhydene.2024.11.346. 2024/12/27/.
[16] Han Y, Liang J, Zou S, Wang S, Gu M. Kinetic characteristics of NO formation in gliding arc plasma assisted premixed ammonia/air combustion. Int J Hydrogen Energy 2026;265:156941. https://doi.org/10.1016/j.ijhydene.2026.156941. 2026/09/03/.
[17] Choe J, Sun W, Ombrello T, Carter C. Plasma assisted ammonia combustion: simultaneous NO_x reduction and flame enhancement. Combust Flame 2021;228:430–2. https://doi.org/10.1016/j.combustflame.2021.02.016. 2021/06/01/.
[18] Tang H, Chatziandreou E, Rahn G, Peng B, Sun W. Simultaneous NH/NO PLIF measurements in plasma-assisted ammonia and ammonia/hydrogen swirling flames. Proc Combust Inst 2025;41:105789. https://doi.org/10.1016/j.proci.2025.105789. 2025/01/01/.
[19] Gong K, Liu Y, Zhao H, Wang Z. Review of gliding arc plasma assisted ignition and combustion for gas turbine application. Int J Turbo Jet Engines 2025;42(2):241–59. https://doi.org/10.1515/tjj-2024-0045.
[20] Aravind B, Wang Z, Mashruk S, Lacoste DA, Valera-Medina A. Novel strategy for combustion enhancement of NH_3-air mixture using gliding arc plasma. Proc Combust Inst 2025;41:105848. https://doi.org/10.1016/j.proci.2025.105848. 2025/01/01/.
[21] Wang Z, Aravind B, Mashruk S, Valera-Medina A. Experimental investigation on the effects of gliding arc plasma on the combustion characteristics of air stratified NH3 flames. Energy 2025;336:138413. https://doi.org/10.1016/j.energy.2025.138413. 2025/11/01/.
[22] Rahmani E, Cid N, Kamal MM, Coussement A, Parente A, Lubrano Lavadera M. The influence of MILD-to-flame transition on stabilization, reactive structures, and emissions of NH3/H2 mixtures in a semi-industrial furnace. Combust Flame 2026;284:114687. https://doi.org/10.1016/j.combustflame.2025.114687. 2026/02/01/.
[23] Wang S, Chen J, Elbaz AM, Wang Z, Roberts WL. Effects of fuel-staging and reburning on NOx emissions from NH3/CH4/air swirling flames. Combust Flame 2026;286:114816. https://doi.org/10.1016/j.combustflame.2026.114816. 2026/04/01/.
[24] Liu Z, et al. Towards efficient/low emission NH3 swirl combustion under axially staged regime through oxygen enrichment. Combust Flame 2025;278:114254. https://doi.org/10.1016/j.combustflame.2025.114254. 2025/08/01/.
[25] Hwang S, Lee JW, Sim W, Yang W, Chae T, Kwon OC. Effects of air flow distribution and equivalence ratios for staged combustion in an ammonia burner. Energy 2025;334:137604. https://doi.org/10.1016/j.energy.2025.137604. 2025/10/15/.
[26] Pan W, Yao N, Chen Y, Kang L. Numerical investigation of NOx emission characteristics in air-staged combustion system fueled by premixed ammonia/methane. J Energy Inst 2024;117:101857. https://doi.org/10.1016/j.joei.2024.101857. 2024/12/01/.
[27] Mao X, Zhong H, Liu N, Wang Z, Ju Y. Ignition enhancement and NO_x formation of NH_3/air mixtures by non-equilibrium plasma discharge. Combust Flame 2024;259:113140. https://doi.org/10.1016/j.combustflame.2023.113140. 2024/01/01/.
[28] Wang Z, Aravind B, Mashruk S, Valera-Medina A. Numerical investigation on the combustion characteristics of premixed NH_3-air flames using gliding arc plasma. J Energy Inst 2025;123:102314. https://doi.org/10.1016/j.joei.2025.102314. 2025/12/01/.
[29] Shahsavari M, Konnov AA, Bai X-S, Valera-Medina A, Li T, Jangi M. Synergistic effects of nanosecond plasma discharge and hydrogen on ammonia combustion. Fuel 2023;348:128475. https://doi.org/10.1016/j.fuel.2023.128475. 2023/09/15/.
[30] Alnasif A, Jójka J, Mashruk S, Nagy T, Valera-Medina A. Analysis of the performance of kinetic reaction mechanisms in estimating N_2O mole fractions in 70/30 vol% NH_3/H_2 premixed flames. Fuel 2024;371:131897. https://doi.org/10.1016/j.fuel.2024.131897. 2024/09/01/.
[31] Dong G, et al. Kinetics-based analysis of the gliding arc plasma assisted ammonia decomposition process towards vehicle on-board applications. Chem Eng J 2025;505:159443. https://doi.org/10.1016/j.cej.2025.159443. 2025/02/01/.
[32] Barney BM, et al. Diazene (HN& #xe5fb;NH) is a substrate for nitrogenase: insights into the pathway of N2 reduction. Biochemistry 2007;46(23):6784–94. https://doi.org/10.1021/bi062294s.
[33] Klippenstein SJ, Harding LB, Glarborg P, Miller JA. The role of NNH in NO formation and control. Combust Flame 2011;158(4):774–89. https://doi.org/10.1016/j.combustflame.2010.12.013. 2011/04/01/.